RSC Advances

ROYAL SOCIETY OF CHEMISTRY

www.rsc.org/advances

Cite this: DOI: 10.1039/c0xx00000x

www.rsc.org/xxxxxx

ARTICLE TYPE

Novel Pd-Core–Pd-Ni Shell in Pt Nanocage

Balachandran Jeyadevan[*a], Jhon L. Cuya[a], Yoshinori Inoue[a], Kozo Shinoda[b], Takashi Ito[c], Derrick Mott[d], Koichi Higashimine[d], Shinya Maenosono[d], Takatoshi Matsumoto[b] and Hiroshi Miyamura[a]

Received (in XXX, XXX) Xth XXXXXXXXX 20XX, Accepted Xth XXXXXXXXX 20XX

DOI: 10.1039/b000000x

Novel Ni-Pd nanocubes with a size of a few tens of nm that are encased in Pt cages have been synthesized using a long chain alcohol reduction process for the first time. The unique distribution of Pt atoms in these particles holds the key for designed synthesis of high turnover catalysts for the future.

Introduction

In recent years, strategy initiatives related to the development of alternate functional materials to replace those based on rare earth and precious metals have been sanctioned in developed countries to overcome the limited and geographically constrained supply of these materials. Precious transition metals, such as Pt and Pd have demonstrated their outstanding potentials as catalysts in chemical, electrocatalytic, automotive and many other key industries in the forms of pure metal as well as alloys.[1,2]

Though considerable progress has been made in the preparation of precious transition metal based colloidal nanostructures, research to replace these precious metals with abundantly available alternative elements have not led to any reasonable success. This has forced the researchers to look for methods to optimize their use by alloying, and developing techniques to preserve the resources through recycling. It is well known that alloying with a second metal can significantly improve the catalytic properties of the original metal and the synthesis of multi metallic nanoparticles (NPs) has become a central topic.[3-5] Alloy NP systems such as Pt-Pd, Pd-Ni and Pt-Ni have been given considerable attention.[6-8] As a consequence, enhanced catalytic activity over that of Pt alone has been reported in the case of core–shell structured Pt–Pd NPs,[9] however, the search for techniques that could enable the formation of new structures with high catalytic activity using smaller amounts of Pt is highly pursued. In addition, attempts have also been made to improve the efficiency and selectivity of Pt-based NPs for specific reaction by engineered exposure of specific crystal facets.[10-13]

All the above studies point out that fine control over the composition and surface structures are necessary for the creation of high throughput and cost effective Pt-based nanostructures. On this line of thought, the authors have attempted the synthesis of Pt-based magnetic alloy NPs such as Fe-Pt,[14] Co-Pt[15] and Ni-Pt[16] NPs, which reduces the net amount of platinum and also imparts magnetic properties, which enables the collection of these materials after use and makes the recovery of precious metals possible. In the case of Fe-Pt, for NPs synthesized by the polyol process, deposited on activated carbon and heat-treated to convert to the face-centred-tetragonal structure have been proven to be a possible alternative catalytic electrode material for polymer electrolyte polymer cells.[17] On the other hand, the syntheses of Ni NPs[18] as well as novel cubic-shaped Ni-Pt NPs[16] have also been achieved through alcohol reduction technique. Furthermore, in a preliminary investigation related to the evaluation of the catalytic performance of cubic shaped Ni-Pt NPs in hydrogenation reaction of 1-octene to octane, $Ni_{91}Pt_9$ NPs (10 nm cubes) performed comparably to the Pt (3.5 nm) metal NPs, when the specific surface area is taken into consideration.

The similarity of properties such as atomic radius, crystal structure, electronegativity between Pt and Pd and the use of these metals as catalysts in the automobile industry for the enhancement in the carbon dioxide and hydrocarbon activities, motivated the synthesis of Ni-Pd-Pt NPs by extending the already established process for the preparation of Ni-Pt NPs to the synthesis of cubic shaped NPs consisting of Pt, Pd and Ni metals. Here, we report the synthesis of novel Pd-core-Pd-Ni shell in Pt nanocage particles, which looks very promising for applications in the field of catalysts.

Experimental Section

Materials

Nickel (II) acetate tetrahydrate [$Ni(CH_3COO)_2{\cdot}4H_2O$, 98%], dihydrogen hexachloroplatinate hexahydrate ($H_2PtCl_6{\cdot}6H_2O$, 98.5%) and palladium acetylacetonate [$Pd(C_5H_7O_2)_2$, 99 %] were purchased from Sigma-Aldrich and used as the metal sources. Solvents such as 1-heptanol (98%), methanol (99.8%), 2-propanol (99.9 %), 1-octene (99.9 %), octane (98.0 %), toluene (99.5%), and oleylamine [$CH_3(CH_2)_7CH{=}CH(CH_2)_7CH_2NH_2$, 70%] were purchased from Wako Pure Chemicals Ltd., Japan. The commercially available reagents were used without further purification.

Synthesis of Ni-Pt-Pd nanoparticles

In a typical procedure to synthesize Ni-Pd-Pt NPs, 3.8 mM nickel salt was totally dissolved in 5 mL methanol using ultrasonication. The above solution was mixed with 100 mL 1-heptanol

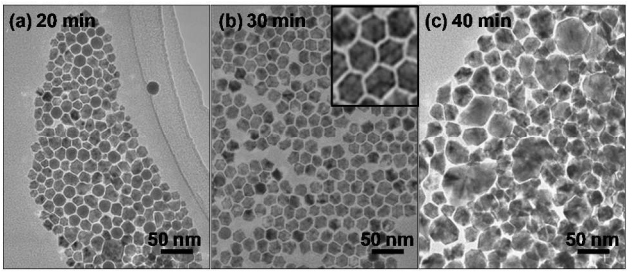

Fig. 1 TEM micrographs of Ni-Pd-Pt NPs sampled at reaction durations (a) 20, (b) 30 and (c) 40 minutes.

containing 42 mM oleylamine, 0.1 mM $Pd(C_5H_7O_2)_2$ and 0.85 mM $H_2PtCl_6{\cdot}6H_2O$, then, heated at 170 °C for 40 min. The resulting NPs were collected by using a magnet. Then, the NPs were washed with a mixture of methanol and toluene in order to remove unreacted compounds and excess oleylamine. Finally, the NPs were redispersed in toluene.

Characterization

The powder diffraction (XRD) patterns of the samples were analyzed using the X-ray diffractometer (XRD, Philips-Xpert) with Cu Kα-radiation to characterize the crystallographic phases present in the powder. The size and morphology of the particles were analyzed by using transmission electron microscope (TEM, Hitachi H8100) operated at 200 kV. The samples for the TEM measurements were prepared by depositing toluene dispersed Ni-Pt-Pd particles on the amorphous carbon-coated grids. In addition, high angle annular dark field (HAADF) microscopy coupled with STEM as well as energy dispersive spectroscopy (EDS) elemental mapping were performed on a JEOL JEM-ARM200F instrument operated at 200 kV with a spherical aberration corrector; the nominal resolution was 0.8 Å. STEM-HAADF imaging and EDS mapping analyses allow us to clearly visualize the relative positions of Ni, Pd and Pt within the individual Ni-Pd-Pt alloy NPs.

In order to analyze the local atomic environmental structure around certain element, the XAFS spectrum of the sample for the Pt L_3 absorption edges was recorded using an in-house X-ray absorption spectrophotometer, namely, Rigaku R-XAS Looper. In the spectrometer, the demountable X-ray tube with Mo target as the white X-ray source and the Si(400) Johansson-type bent single crystal as the monochromator crystal were used. The experiments at Pt L_3 absorption edges were carried out in the transmission mode using the samples diluted with BN powder and pelletized and in the fluorescence yield mode using the samples pressed without dilution, respectively. The data processing of the measured X-ray absorbance spectra was carried out by using the program REX2000 ver. 2.5.9 produced by Rigaku.

Local chemical environment of constituent atoms was carried out on a Shimadzu Kratos AXIS-ULTRA delay-line detector high-performance X-ray photoelectron spectroscopy system. The XPS measurement details are as follows: Photoelectrons were excited by monochromated Al Kα radiation. Detection was performed with a delay-line detector and a concentric hemispherical analyzer. The X-ray tube was operated at 150 W. The pass energy of the concentric hemispherical analyzer was 20 eV for narrow-scan spectra. The analyzed area on the specimen surface was 300–700 mm^2 and was located in the center of the irradiated region. For the sample preparation, the precipitated NPs were deposited on carbon tape and dried in air. The instrument was operated at a vacuum level of 1×10^{-8} torr.

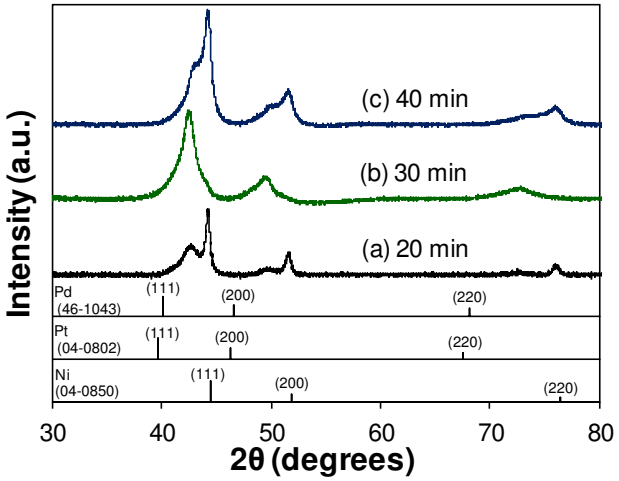

Fig. 2 XRD patterns of Ni-Pt-Pd NPs samples withdrawn after (a) 20, (b) 30 and (c) 40 minutes of reaction at 170 °C.

The catalytic properties of Ni-Pd-Pt NPs were examined through the hydrogenation reaction of 1-octene to octane. In this regard, specific amount of Pt, Ni-Pd-Pt or acid treated Ni-Pd-Pt NPs were introduced in a three-necked glass round flask together with 50 mL 2-propanol and 5 mL 1-octene. The solution was heated at 83 °C under a constant flow of pure H_2 gas (99.999 %) and mechanical stirring (300 rpm). After refluxing for 2 h, the solution was cooled and then analyzed by gas chromatograph to evaluate the amount of octane conversion.

Results and Discussion

To monitor the formation of NPs, sampling was done at different durations once the reactants reached the specified temperature. Fig. 1 shows the TEM micrographs of the samples taken at 20, 30 and 40 minutes at the reaction temperature of 170 °C. Though the NPs were not so uniformly shaped in the sample collected after a reaction time of 20 minutes, they became very uniform and cubically shaped after 30 minutes of reaction. However, when the reaction progressed further, the NPs became irregular in shape and also non-uniform in size. At this point, we speculated the precipitation of different crystal phases along the period of time. Thus, we decided to structurally analyze these NPs using X-ray diffraction (Rigaku RINT2000), using Cu-Kα radiation as the incident X-ray source. The results of the measurements are shown in Fig. 2. XRD patterns show the sequential shift to the right in the face-centred-cubic structure peaks corresponding to the Pt/Pd(111) peak. The main peak of Pt/Pd shifts toward higher angle as the reaction progresses. This is due to the increase in the Ni composition in the Ni-Pd-Pt alloy NPs, which is well-known as the decrease in lattice constant by alloying of Pt/Pd with Ni. The relationship between the lattice constants derived from the XRD ($Ni_{0.59}(PdPt)_{0.41}$) and the composition of the NPs evaluated from the EDS analysis ($Ni_{0.72}(PdPt)_{0.28}$) shows a positive deviation from the ideal Vegard's law. On the other hand, in the

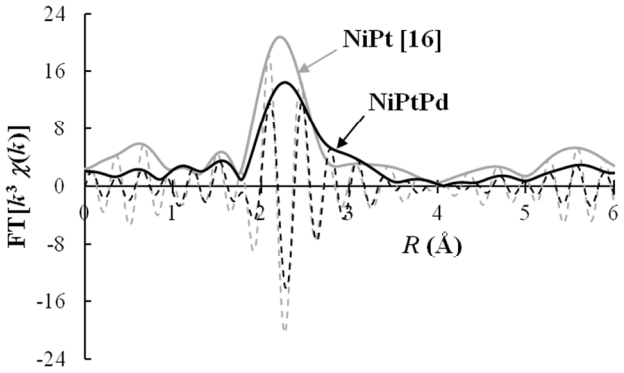

Fig. 3 Fourier Transforms of k^3 weighted EXAFS spectra measured at Pt L_3 absorption edge for the samples of Ni-Pd-Pt (this work, reaction time was 30min) and Ni-Pt[16].

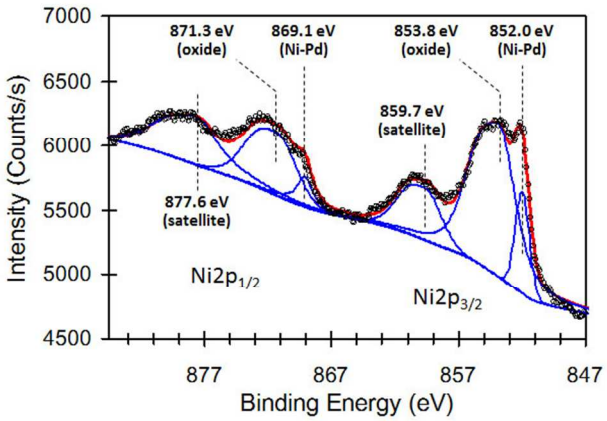

Fig.4 High-resolution Ni 2p XPS core-level spectrum of the Ni-Pd-Pt sample synthesized at 170 ˚C for 30 minutes.

case of the Ni(111) peak a slight shift to the left is observed for the sample taken after 20 minutes of reaction time, however, within 30 minutes the diffraction peaks corresponding to both Ni and Pd/Pt merge and a single peak suggesting the formation of Ni-Pd-Pt alloys was observed. The lattice constant of the alloy was calculated from the XRD pattern as approximately 0.367 nm. In this alloy phase, the nearest neighbouring interatomic distance is 0.260 nm. After 40 minutes of reaction, in addition to the peak corresponding to the Ni-Pd-Pt alloy, the reappearance of the Ni(111) peak was observed. This was due to the reduction of Ni ions remained in the system and their subsequent precipitation on the surface of cubic-shaped particles. Consequently, the particles lost their shape and became very irregular.

From the above results, we could postulate that at the initial stages of the reaction, Ni, Pd and Pt alloyed and after 30 minutes of reaction, the Ni atoms that remained in the solution began to precipitate preferentially on the surface of the alloyed NPs. The proposed reaction scheme also explains the reason for the shape and size of the NPs observed after 40 minutes of reaction in Fig. 1 (c). Most of the particles synthesized under the optimum conditions are nearly cubic (see the inset in Fig. 1b). However, when the lengths of the particles are not exactly the same, then they look different and the projected figure becomes complicated since the particles are standing on their corners. The HRTM does not confirm the formation of twining or intergrowth. Though the morphological and structural analyses have revealed the formation and growth mechanisms, the local atomic environment within the NPs is yet to be resolved. Thus, in order to analyze the local atomic environmental structure around Pt atoms, the XAFS spectrum of the sample for the Pt L_3 absorption edge was recorded using an in-house X-ray absorption spectrometer (Rigaku R-XAS Looper) housing a demountable X-ray tube with Mo target as the white X-ray source and Si(400) Johansson-type bent single crystal as the monochromator. The experiments were carried out in the fluorescence yield mode using the pressed samples.

FEFF 8.20 code was used for the theoretical calculation of the backscattering amplitudes and phase shift parameters of scattering photoelectrons and REX2000 ver.2.5.9 program (Rigaku co.) was used for analysis of the measured EXAFS spectrum. The correlation peak for nearest neighbouring pair was corresponding to Pt-Ni in the Ni-Pt alloy[16]. In the Ni-Pd-Pt alloy, the first nearest neighbour corresponds to Pt-Ni as in case of the Ni-Pt alloy. The obtained distance of 0.258 nm corresponded well to the value calculated from the XRD pattern. The Fourier transforms of measured k^3 weighted EXAFS spectrum for the Ni-Pd-Pt alloy sample is shown in Fig. 3 along with that for the Ni-Pt alloy [ref. 16]. In the Pt L_3 Fourier transform for Ni-Pd-Pt sample, a small atomic pair correlation is indicated at further distance as shoulder of the nearest neighbouring Pt-Ni pair correlation peak. This correlation is not considered as the second nearest neighbouring one in the FCC alloy since the observed distance is too much shorter than 0.367 nm even after taking the shift of peak position in the Fourier transform due to the phase shift of oscillation in the EXAFS spectrum into account. Thus, from the correlation shoulder position, this is considered to be the consequence of Pt-Pt (0.277 nm in pure platinum) or Pt-Pd (0.275 nm in PtPd alloy) in Ni-diluted alloy. Considering the results obtained from elemental distribution mapping shown in Fig. 5, the closer correlation peak and the further correlation shoulder in the Fourier transform are corresponding to the nearest neighbouring Pt-Ni pair in Ni-Pt alloy located at the shell area of particle and Pt-Pt pair in Pt-rich alloy located at edge of particle, respectively.

To obtain additional information regarding the local chemical environment of constituent atoms, we performed X-ray photoelectron spectroscopy (XPS) analysis. XPS analysis was carried out on a Shimadzu Kratos AXIS-ULTRA delay-line detector high-performance XPS system. Fig. 4 shows the high-resolution Ni2p XPS core-level spectrum of the Ni-Pd-Pt alloy NPs. The background subtraction was done using the Shirley method. The shift of the binding energy (BE) scale due to charging was corrected by internal referencing of the C1s peak (284.4 eV). The Ni2p core levels are split into $2p_{1/2}$ and $2p_{3/2}$ spin-orbit pairs. To look at the Ni2p XPS spectrum in more depth, the Ni2p spectrum was deconvoluted into three different Ni species including Ni-Pd metal/alloy, oxide/hydroxide, and structure with an intense satellite signal at high BE adjacent to the main peaks, which can be attributed to multi-electron excitation. After these shake-up peaks are taken into account, the $Ni2p_{3/2}$ XPS peaks at the binding energies of 852.0, 853.8, and 859.7 eV were assigned to Ni-Pd alloy,[19] Ni oxide/hydroxide, and satellite, respectively. Note that the BEs of Pd3d and Pt4f show that Pd

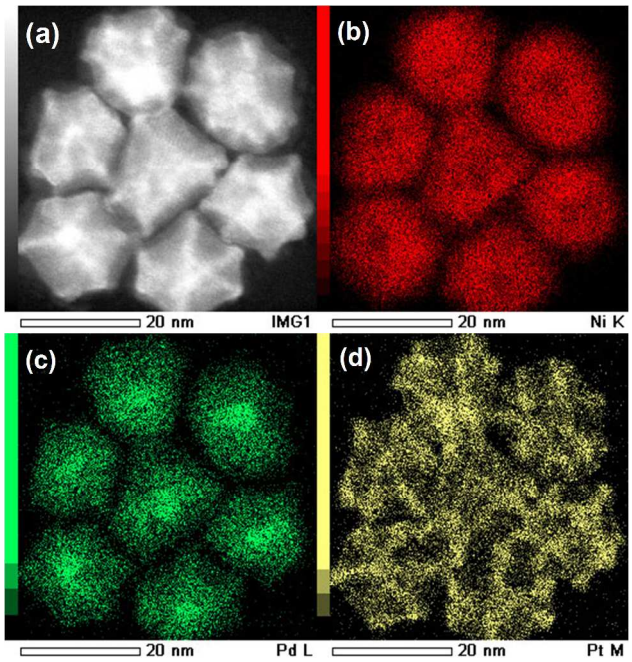

Fig. 5 (a) STEM-HAADF image and (b-d) EDS elemental mapping images of the Ni-Pd-Pt alloy NPs. (b) Ni K edge, (c) ,Pd L edge. and (d) Pt M edge.

and Pt are present in the zero valent metallic state in the Ni-Pd-Pt alloy NPs. (Fig. S1)

Though considerable information was obtained through the above mentioned techniques, the distinction between behavior of Pt and Pd was not possible and also information related to their role in the formation or their distribution within the particles was not obtained. Thus we attempted observation of the atomic distribution using the scanning transmission electron microscopy (STEM). High angle annular dark field (HAADF) microscopy coupled with STEM as well as energy dispersive spectroscopy (EDS) elemental mapping were performed on a JEOL JEM-ARM200F instrument operated at 200 kV with a spherical aberration corrector; the nominal resolution was 0.8 Å. STEM-HAADF imaging and EDS mapping analyses allow us to clearly visualize the relative positions of Ni, Pd and Pt within the individual Ni-Pd-Pt alloy NPs in Fig. 5 Since the heavier Pt atoms (atomic number, Z=78) give rise to a brighter image than the lighter Ni (Z=28) and Pd (Z=46) atoms in the dark field image, the Pt cage appears brighter than the Ni-Pd core. When comparing this image to the EDS elemental map, it is shown that a majority of Pt atoms exist at the vertices and sides of the cubic NPs. In addition, it is also shown that the cubic Ni-Pd core consists of a Pd-rich center and Ni-Pd alloy outer layer. The spatial distribution of Pd within the NPs suggests that Pd ions are preferentially reduced compared to Pt and facilitates heterogeneous nucleation and subsequent co-reduction of Ni and Pd leading to the formation of uniform Ni-Pd alloy shell around the Pd core. Surprisingly, Pt ions are not reduced prior to Pd or even Ni. Except for a recent report on the synthesis of PtPd alloy NPs,[6] the one-pot reduction of Pt and Pd is often claimed to form core-shell NPs. In contrast, Pd alloys preferentially with Ni over Pt and this supports the vast amount of literature on Pd-Ni alloy formation.[7,20] Thus, Pt ions are not allowed to be incorporated in Ni-Pd alloy and finally get reduced on the active sites of the

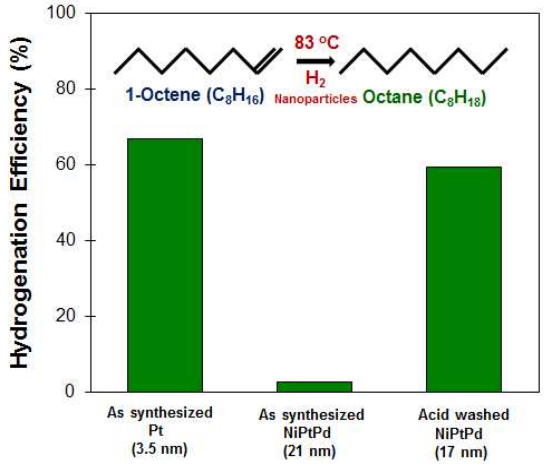

Fig. 6 The conversion rates of 1-octene to octane hydrogenation reaction, considering a similar weight of metal catalysts, for (a) as-synthesized Pt, (3.5 nm) as-synthesized Ni-Pd-Pt (21 nm) and (c) acid-treated Ni-Pd-Pt (17 nm)

Ni-Pd cubes, such as the corners and edges. However, the reason for the absence of separate Pt NPs is not clear at present. Furthermore, the driving force for the formation of the cubic shape of the NPs in Ni-Pd-Pt ternary systems also needs to be investigated. Since the Ni-Pt NPs also formed cubic shape, we carried out STEM analysis to study the distribution of Pt in these NPs. Here again, we were able to see the presence of Pt in the edges and corners of the cubes (Fig. S2). In contrast, the Ni NPs formed in the absence of Pt are very irregularly shaped and large. This suggested that Pt atoms play an important role in facilitating the formation of cubic shaped NPs. Another noteworthy observation was that the concentration of Pt atoms deposited on the cubes was higher in the case of Ni-Pd-Pt than Ni-Pt. This suggests that the presence of Pd atoms make the corners and edges of the cube more active. Likewise, it should be noted that the reduction of Pt ions is delayed when oleylamine was introduced to the system. When the synthesis of Pt particles was attempted in the presence and absence of oleylamine, the formation of Pt nanoparticles was observed at 393K for the oleylamine–free case. On the other hand, in the presence of olylamine the Pt particle began to form at temperatures higher than 343 K. In contrast, the formation of Ni and Pd particles was not influenced by the presence of oleylamine. These experimental results partially explain the formation of novel structure observed in this study. However, further study is necessary to fully understand the formation mechanism of this novel Pd-core-Ni-Pd shell in Pt nanocage.

The potential of these particles as catalyst was attempted by comparing the conversion rates in the hydrogenation of 1-octene to octane reaction. The results are shown in Fig. 6. Here, the conversion rates of 1-octane to octane for 3.5 nm Pt was very high when Ni-Pd-Pt particles were used in the as-synthesized state. However, their performance became comparable with Pt nanoparticles when the Ni-Pd-Pt particles were washed with acid. The reason for the above was investigated and the presence of oleylamine has been confirmed in the as-prepared samples (Fig. S3 and S4). However, washing these particles with either with a mixture of toluene and methanol or nitric acid helps to remove

the oleylamine molecules considerably and make them suitable for catalytic measurements (Fig. S3 and S4). In addition, the removal of excess nickel metal deposited on the surface of the cubes also would have contributed to improvement in the conversion rate. As shown in Fig. 1 (c), when the reaction time is prolonged, the nickel ions that remained in the solution begin to deposit on the surface of the cubes and inhibit the exposure of Pt atoms on the edges and corners of the cube.

We believe that the elucidation of the formation mechanism of these novel nanostructures will allow us to control the amount of Pt atoms that deposit on the edges and corners of the cube and subsequently influence the catalytic or other functional properties of these particles. The elucidation of the formation mechanism of bimetallic Ni-Pt particles by the authors, which will be communicated soon will pave the way for improved design of multi-functional Ni-Pd-Pt particles.

Conclusions

We have reported the synthesis of novel Pd-core-Ni-Pd shell in Pt cage NPs. Though the structural, morphological and atomic distributions of these NPs are exposed, factors that facilitate the formation of such unique nanostructure are yet to be determined fully and further investigation would pave the way for designed synthesis of multi-functional particles with novel structures. The experiments to elucidate the crystal formation mechanism as well as to determine the potential of these particles in various fields are in progress.

Acknowledgments

This study was supported by Grant-in Aid for Basic Research (B) and 22310064 and Challenging Exploratory Research 25600028 from the Ministry of Education, Science, Culture and Sport of Japan.

Notes and references

[a]*Department of Material Science, The University of Shiga Prefecture, 2500 Hassaka Cho, Hikone 522-8533, Shiga, Japan. Email; jeyadevan.b@mat.usp.ac.jp;Fax:+81 749 28 8486; Tel:+81 749 28 8352.*
[b]*Institute of Multidisciplinary Research for Advanced Materials, Tohoku University, Sendai, Japan. E-mail: shinoda@tagen.tohoku.ac.jp; Fax:+81 22 217 5624; Tel: +81 22 217 5624.*
[c]*Frontier Research Institute for Interdisciplinary Sciences, Tohoku University, Sendai, Japan. E-mail: ito@cir.tohoku.ac.jp; Fax:+81 22 217 5624; Tel: +81 22 217 5624.*
[d]*School of Material Science, Japan Advanced Institute of Science and Technology, 1-1 Asahidai, Nomi, Ishikawa Prefecture, 923-1211, Japan. E-mail: shinya@jaist.ac.jp; Fax:; Tel: +81 761 51 1611.*

1. R. R. Barefoot, J. C. Van Loon, *Anal. Chim. Acta*, 1996, **334,** 5.
2. J. Lipkowski, P. N. Ross, Electrocatalysis, Wiley-VCH, New York, 1998.
3. A. Serov, C. Kwak, *Appl. Catal*., B 2009, **90**, 313.
4. S. I. Lim, I. Ojea-Jimenez, M. Varon,E. Casals, J. Arbiol, V. Puntes, *Nano Lett*. 2010, **10**, 964.
5. V. R. Stamenkovic, B. Fowler, B. S. Mun, G. Wang, P. N. Ross, C. A. Lucas, N. M. Markovic, Science 2007, **315**, 493.
6. X. Huang, Y. Li, Y. Li, H. Zhou, X. Duan, and Y. Huang, *Nano Lett*. 2012, **12**, 4265.
7. K. Lee, S. W. Kang, S-U. Lee, K-H. Park, Y. W. Lee, and S. W. Han, *ACS Appl. Mater. Interfaces*, 2012, **4**, 4208.
8. C. Cui, L. Gan, H-H. Li, S-H. Yu, M. Heggen and P. Strasser, *Nano Lett*. 2012, **12**, 5885.
9. L. Liu, G. Samjeske, S. Nakamatsu, O. Sekikawa, K. Nagasawa, S. Takao, Y. imaizumi, T. Yamamoto, T. Uruga, and Y. Iwasawa, *J. Phys. Chem. C*, 2012, **116**, 23453.
10. J. Chen, B. Lim, E. P. Lee, Y. Xia, *Nano Today* 2009, **4**, 81.
11. T. S. Ahmadi, Z. L.Wang, T. C. Green, A. Henglein, M. A. El-Sayed, *Science* 1996, **272**, 1924.
12. R. Narayanan, M. A. El-Sayed, *J. Phys. Chem. B* 2005, **109**, 12663.
13. K. M. Bratlie, H. Lee, K. Komvopoulos, P. Yang, G. A. Somorjai, *Nano Lett.* 2007, **7**, 3097.
14. B, Jeyadevan, K. Urakawa, A. Hobo, N. Chinnasamy, K. Shinoda, K. Tohji, D. D. J. Djayaprawira, M. Tsunoda, M. Takahashi, *Jpn. J. Appl. Phys*., 2003, **42**, L350.
15. C. N. Chinnasamy, B. Jeyadevan, K. Shinoda, K. Tohji, *J. Appl. Phys.*, 2003, **93**, 7583.
16. Jhon L. Cuya Huaman, S. Fukao, K. Shinoda and B.Jeyadevan, *CrystEngComm*., 2011, **13**, 3364.
17. T. Itoh, M. Uebayashi, K. Tohji, and B. Jeyadevan, *Electrochemistry.* 2010, **78**, 157.
18. Jhon L. Cuya Huaman, N. Hironaka, S. Tanaka, K. Shinoda, H. Miyamura, B. Jeyadevan, *CrystEngComm*, 2013, **15**, 729.
19. F. U. Hillebrecht, J. C. Fuggle, P. A. Bennett, and Z. ZoLierek, *Phys. Rev. B*, 1983, **27**, 2179.
20. Y. Wu, D. Wang, P. Zhao, Z. Niu, Q. Peng, Y. Li, *Inorg. Chem*., 2011, **50**, 2046.